

A Deep Learning Approach to Within-Bank Fault Detection and Diagnostics of Fine Motion Control Rod Drives

Ark Ifeanyi¹, Abhinav Saxena², and Jamie Coble³

^{1,3} University of Tennessee-Knoxville, Knoxville, TN, 37996, USA

aifeanyi@vols.utk.edu

jamie@utk.edu

² GE-Research, Niskayuna, NY, USA

asaxena@ge.com

ABSTRACT

Control rod motion is one of the primary means of regulating the rate of fission in a nuclear reactor core to ensure safe and stable operation. Reactor power distribution and thermal power output can be fine-tuned by adjusting the control rod position. For high-precision control of rod movements, Fine Motion Control Rod Drives (FMCRDs) are often used. The operation of FMCRDs provides a unique opportunity to implement condition monitoring related to the intermittency of motion and the use of control rod banks. This research sets out to detect three types of faults in an electrically driven FMCRD. In addition to detecting faults, this work will attempt to determine both the type of fault and the source of each fault, completing the fault detection and diagnostics (FDD) pipeline on a scarcely researched system. The three types of faults to be investigated are short-circuit faults, ball screw wear faults, and ball screw jam faults. This is a potential advancement to the within-bank FDD of this specific drive system intended for deployment in an advanced nuclear reactor plant. Using encoder-decoder structured convolutional neural networks and autoencoders, the three tested faults were confidently detected and isolated as well as reasonably diagnosed by monitoring the FMCRD servomotor torque.

1. INTRODUCTION

Control rods (CRs) serve a crucial function in the management of the thermal power produced in a nuclear reactor core. By absorbing neutrons, an inserted CR slows the rate of fission. As the CR is extracted, fewer neutrons are absorbed and the rate of fission increases. This insertion and withdrawal is usually achieved with a driving mechanism. The fine motion control rod drive (FMCRD) provides precise con-

trol of CR position. The BWRX-300 design by GE-Hitachi uses servomotors for FMCRDs, a change from the primarily hydraulically-driven CR drives in current boiling water reactors (BWRs).

Fig. 1, illustrates a representative reactor core layout for typical operations of control rod banks (Louis et al., 2021). In this illustration, taken from an Evolutionary Power Reactor (EPR) from the US EPR projects, the nuclear core has two-hundred and forty-one (241) fuel assemblies (total squares in the grid) with seven (7) distinct assembly designs where each assembly has two-hundred and sixty-five (265) fuel rods. Individual control rods are distributed within a fuel assembly to form a group (bank). Individual rods in a control rod bank are independently controlled and, hence, not connected physically. While they are in proximity and move together as a unit when inserted or withdrawn, each rod operates independently within the fuel assembly to control the rate of nuclear reaction. The EPR in Fig. 1 further shows how different banks can be grouped into clusters to provide flexibility and redundancy in controlling the reactor. The EPR contains eighty-nine (89) banks grouped into seven clusters (control – 4; shutdown – 3), one for each assembly design. Different banks can be inserted or withdrawn in overlapping patterns to maintain uniform power distribution and avoid localized power peaks. This overlap ensures smooth reactivity control and prevents sudden changes in power levels. Certain banks are designated as shutdown banks and are specifically reserved for rapidly shutting down the reactor in case of emergencies. SMR designs such as the BWRX-300 used as a reference in this work include a similar arrangement of control rod banks which are prime candidates for health monitoring to ensure performance, reliability, and safety.

FMCRD operation introduces unique challenges and opportunities for condition monitoring and health assessment. First a challenge: CR motion is intermittent (that is, CRs spend

Ark Ifeanyi et al. This is an open-access article distributed under the terms of the Creative Commons Attribution 3.0 United States License, which permits unrestricted use, distribution, and reproduction in any medium, provided the original author and source are credited.

<https://doi.org/10.36001/IJPHM.2024.v15i1.3792>

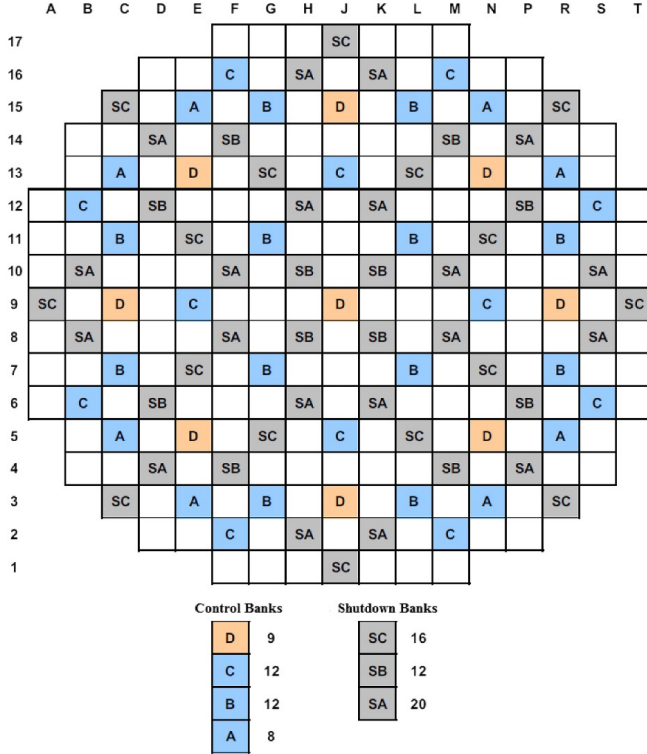


Figure 1. Rod cluster control assembly pattern (Louis et al., 2021).

much of their time in a stationary position and only move when commanded in response to changing reactor conditions) and movement typically occurs over short time intervals. While the CR is in a stationary position, the servomotor will not provide any data that could indicate its condition. Second an opportunity: CRs are moved in banks (groups of two or more rods) and these banks are distributed throughout the reactor core to manage the power profile. For the BWRX-300, this means that several FMCRDs are commanded to make the same adjustment in concert. This coordinated motion across multiple FMCRD servomotors provides a local population of systems that should be working effectively identically (see Fig. 8). We propose to leverage this coordinated operation to monitor the health of each servomotor in the bank, hence, the "within-bank" analyses.

This research aims to use deep neural networks to detect, isolate, and diagnose three types of faults within nuclear reactor control rod drive (CRD) mechanisms. These mechanisms are important for accurately controlling the insertion level of the control rods, which in turn regulates the thermal power output of the reactor, allowing dynamic operations and ensuring safety.

Two sensed properties were analyzed: the position of the CRs over time and the torque being delivered by the servomotor. An autoencoder is trained using these two types of data col-

lected from a healthy FMCRD system. This autoencoder then attempts to recreate data for another healthy system. The reconstruction error of the healthy system serves as a baseline when running a faulty system; the anomalies should lead to substantially higher reconstruction errors, indicating the presence of a fault. By analyzing the reconstruction error of each rod/servomotor within the bank, we can detect not only that there is a faulty rod/servomotor combination in the bank, but which rod's FMCRD is not functioning normally. The data used in this study were acquired from a simulated FMCRD model, which consists of a servomotor and a ball screw system that are interconnected (Subramanian et al., 2023). The described model was used to generate data for this work separate from those described in the reference. The three types of simulated faults are short circuits (electrical), ball screw wear, and ball screw jam. The ball screw is a part of the drive mechanism that is magnetically coupled to the motor and causes linear rod motion from the rotation of the motor rotor. The wear and jam faults are both mechanical faults, the former simulated as a gradual load increase and the latter simulated as an instant large increase in load.

1.1. Motivation and Literature Review

Due to their compact size and flexible operations, small modular reactors (SMRs) are currently attracting research interests, private sector funding, and state support, but none is currently operational in the US with the reported first planned operation in 2029 (AP News, Accessed: Oct. 19, 2023; Energy.gov, Accessed: Oct. 19, 2023). The proposed drive mechanism in GE-Hitachi's BWRX-300 SMR is an electrically driven FMCRD. Flexible operations of the SMRs would require heavy usage of their drive mechanisms which makes the mechanisms key maintenance targets. The ability to detect faults easily and accurately in these motors can significantly contribute to the economic viability of the SMR. In addition, reduced SMR operation and maintenance (O&M) costs can firmly support the role of the world nuclear fleet in providing global energy security.

The results of this work can be of immense relevance in the maintenance and reliability of nuclear plants. Real-time monitoring of the equipment becomes helpful in making predictive maintenance more efficient. Outputs of the fault detection models may also be passed as inputs to prognostics models for the estimation of the remaining useful life of the plant. Beyond these, any machinery with rotating parts, intermittent operations, and similar fault behaviors such as the yaw control of wind turbines may be able to employ the approach explored in this work.

Although some research efforts have gone towards fault detection and diagnostics (FDD) of control rod drives (CRDs) (Jie et al., 2019), only a few focus on FMCRDs. One published work for fault detection in FMCRDs monitored dis-

placement and used a purely statistical thresholding approach for anomaly detection. A threshold was placed on the average difference between the demanded positions and the actual positions of the rods in a bank. This average difference in a bank of rods was expected to vary between healthy and faulty banks (Fullilove et al., 2022). In that attempt, only one fault type (short-circuit) was detected (Fullilove et al., 2022). Another more recent work applied principal component analysis (PCA) to the anomaly detection of FMCRDs where T-squared statistics and Q-statistics were employed for anomaly detection (Ifeanyi et al., 2023). In this second paper, the observation period had to be increased to include more data points in the training data to make detection and isolation possible (Ifeanyi et al., 2023). The approach in this current paper aims to learn complex relationships between variables and potentially detect all the fault types with fewer observations in the training data and a limited number of samples. Additionally, this paper completes the FDD cycle of fault detection, isolation, and diagnostics on this highly underrepresented system in the literature.

Several anomaly detection techniques have been used over the years including classification-based, clustering-based, nearest neighbor-based, and statistical approaches (Chandola & Banerjee, n.d.). For this paper, fault detection will be done by classifying a bank of control rods as faulty or healthy. Anomaly detection can be done with both traditional machine learning techniques and more advanced deep learning methods (Chalapathy & Chawla, 2019). In the application of deep learning, autoencoders are the most widely used architectures in anomaly detection and fault isolation with regard to prognostics and health management (PHM) (Rezaeianjouybari & Shang, 2020). Autoencoder reconstruction has been used for anomaly detection in industrial motors (Givnan et al., 2022) and variational autoencoders have been applied to detect anomalies in electric drives (Shim et al., 2022). Due to their wide acceptance and high success rates in similar applications, a variant of the autoencoder was the choice architecture in this work for fault isolation. With regard to fault detection, a specifically structured deep learning classification model was employed in this work. Deep learning models have the added advantage of not strictly requiring feature engineering to uncover complex relationships (Ahmed et al., 2023). Furthermore, autoencoders are especially good at extracting useful information due to the constraints of the code layer (Chen et al., 2018; Goodge et al., 2021) and this is required for the investigated unique application given the intermittent operations of the servomotors explained in section 2 and the limited number of samples available for this work. 1-dimensional convolutional neural network (1D-CNN)-based autoencoders were used in place of the regular fully connected layer-based autoencoders to retain the temporal relationships in the input data. The suggested method's capacity to simultaneously account for the temporal dependency of each sensor variable

and the nonlinear correlations between several sensor variables is one of its main advantages over the aforementioned statistical methods.

With respect to fault diagnostics of motors, there are many approaches that have been employed in the past but the most common, by far, is motor current signature analysis (MCSA). In MCSA the properties of the current signal of the motor are analyzed and referenced with established behaviors for different fault types to classify the investigated fault (Mehala & Dahiya, 2007; Jung et al., 2006; Messaoudi & Sbita, 2010). The drawback of this approach is that it becomes difficult to classify faults without previously established behaviors. In addition, more than one fault can have very similar characteristics, leading to an increased chance of incorrect diagnosis. On top of that, it requires the monitoring of motor current, therefore, making classification impossible where the current signals are not monitored. As a result of these challenges, more recent techniques have focused on the application of neural networks in the area of induction motor fault diagnostics (Kowalski & Orlowska-Kowalska, 2003). For these techniques, other signals such as vibration signals may be investigated for the purpose of fault diagnostics. Other researchers have tried to diagnose motor faults by applying Fuzzy Logic-based techniques either as precursors to other diagnostic techniques or as the main diagnostics algorithm (Zhongming & Bin, 2000). Not much work was found for diagnostics in FMCRDs and no known published work has discussed application in within-bank analysis. In this work, a 1D-CNN-based classification model was applied to attempt diagnostics within banks of FMCRDs. 1D-CNNs have proved useful for fault diagnosis where the input signals are sequences (Tang et al., 2020; Eren et al., 2019; Azizjon et al., 2020), hence, their application throughout this paper.

This paper presents the development and evaluation of a condition monitoring framework for monitoring the health of each FMCRD servomotor in a bank of CRs. Section 2 describes the data used in considerable detail whereas section 3 takes a deep dive into the various methods employed to achieve the set goals of this research. Section 4 outlines the outcomes of these different approaches and discusses their implications. Finally, section 5 gives a summary of the work and proposes areas for future investigation. The term 'faulty rods' used throughout this paper more appropriately refers to the faulty drive mechanisms of the control rod drive system. Although this terminology may not precisely reflect the technical aspect, it has been retained to aid readers' comprehension and facilitate their visualization of the system's operation.

2. DATA SET

The data for this project are derived from a Matlab Simulink model of an FMCRD (Fullilove et al., 2022). These data show the responses of control rod banks to position change

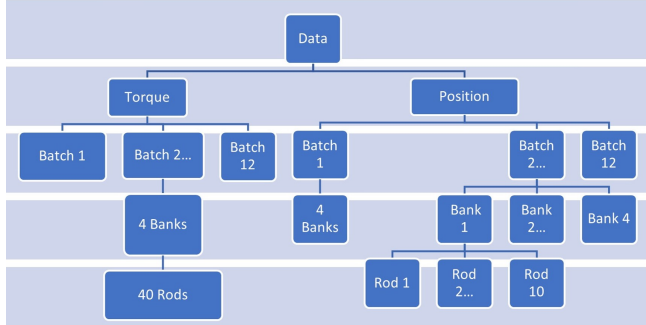


Figure 2. Hierarchical structure of the input data.

demands during a ten-second maneuver (see Fig. 3). The electromagnetic torques in Newton-meters of the servomotors in the bank are measured as one variable whereas the attained displacements of the rods, in centimeters, are monitored as the second variable. For each variable, there are twelve batches of data (Fig. 2), each with a different motion profile across the observed period. Each batch of data has four banks: one healthy bank of rods and three problematic banks, one for each tested fault type. Each bank has ten rods, with the healthy banks having ten healthy rods and the faulty banks having one faulty rod arbitrarily placed in position '10'. Fig. 2 shows the breakdown of the data with some components deliberately missing because it was intended as a summary. The 'Torque' branch shows the total number of rods and the total number of banks in any batch, even though it was only illustrated for batch '2'. These totals are evenly distributed such that any one bank has ten rods as illustrated on bank '1' of batch '2' in the 'Position' branch.

Furthermore, each rod has five hundred thousand (500,001 including the starting point) observations for each measured parameter for a ten-second maneuver collected at a sampling rate of 50kHz. Sequence data from each bank of ten (10) rods with ten-second sequences (500001 data points) of position or torque is treated as one sample in this work. In other words, the input shape is $(x, 500001, 10)$ where x represents the number of banks (samples). Simulations were run to collect data from forty-eight (48) simulated bank operations, twelve (12) for each of the four (4) health categories: healthy (no fault); short-circuit fault; ramp fault; and step fault.

What constitutes training and test sets varied for the different tasks and will be explained in the appropriate sections. For all test cases with a single fault, the faulty rod was in the same variable index ('10') of the bank for ease of reading, but could realistically appear in any index without impacting the performance of the detection and isolation routines. To demonstrate the independence of the rod position index, the indexes of the faulty rods were varied for the isolation of multiple faults in a bank.

Each batch of the data has a different position demand pro-

file and the profile for the healthy bank of batch '1' is seen in Fig. 3 a) along with the corresponding torque behavior in Fig. 3 c). For brevity, this section specifically discusses the behavior of batch '1', although similar patterns were observed in the healthy banks of all other batches (see Fig. 3 b) and d)). One second into the observation of batch '1', a position change demand was made, and the rods of that bank gradually ascended to the demanded position of around 1.735 cm where an overshoot occurred before settling at the demanded position. As soon as another request to ascend was made at the 5th second, the gradual movement occurred with another equilibrium settling required. These periods where the rods in the bank are moving to achieve the desired position represent the operating periods of the drive mechanism. Since the servomotor only operates for a fraction of the observation period, the data points from the rod position signals with useful information for fault detection are limited, therefore, complicating the FDD tasks. Position demand is instantaneous as shown by the step profile in Fig. 3 whereas actual rod movements are gradual, resulting in a time lag between actual and demanded positions. The torque signal shows that a sharp change in torque is experienced during the transient periods just after a position demand is made and where equilibrium settling is required. These short-duration transient periods highlight where the motors are being called to action and indicate the useful points of torque variations to be monitored for the FDD tasks. Note that Fig. 3 illustrates the key points with a single rod's profile, however, all rods in the healthy bank will have the same profile for both variables leading to overlapping lines as seen in Fig. 8 for position and torque. Fig. 3 b) and d) simply illustrate how these demand profiles vary from batch to batch as a different profile is seen in batch '2' but with similar behaviors and torque-position relationships.

3. TECHNICAL APPROACH

In order to train a model for differentiating between healthy and faulty FMCRDs, first, a model needs to be constructed and the input data needs to be decided. The input data shown in Fig. 2 are the monitored torque and position values of the rods in a bank. The inputs are banks of sequences of position or torque signals as described in section 2. Because of the desire to process the input as a collection of sequences, all the models used for the different tests only had 1D-CNN layers with the output layers chosen based on the tasks to be performed.

3.1. Fault Detection

In this work, detection was treated as a classification task where the input banks were classified as either faulty or healthy. An encoder-decoder (E-D) structure (see Fig.4) was selected for this task. E-D structures are popular for applications that require constraining the network to potentially force the learn-

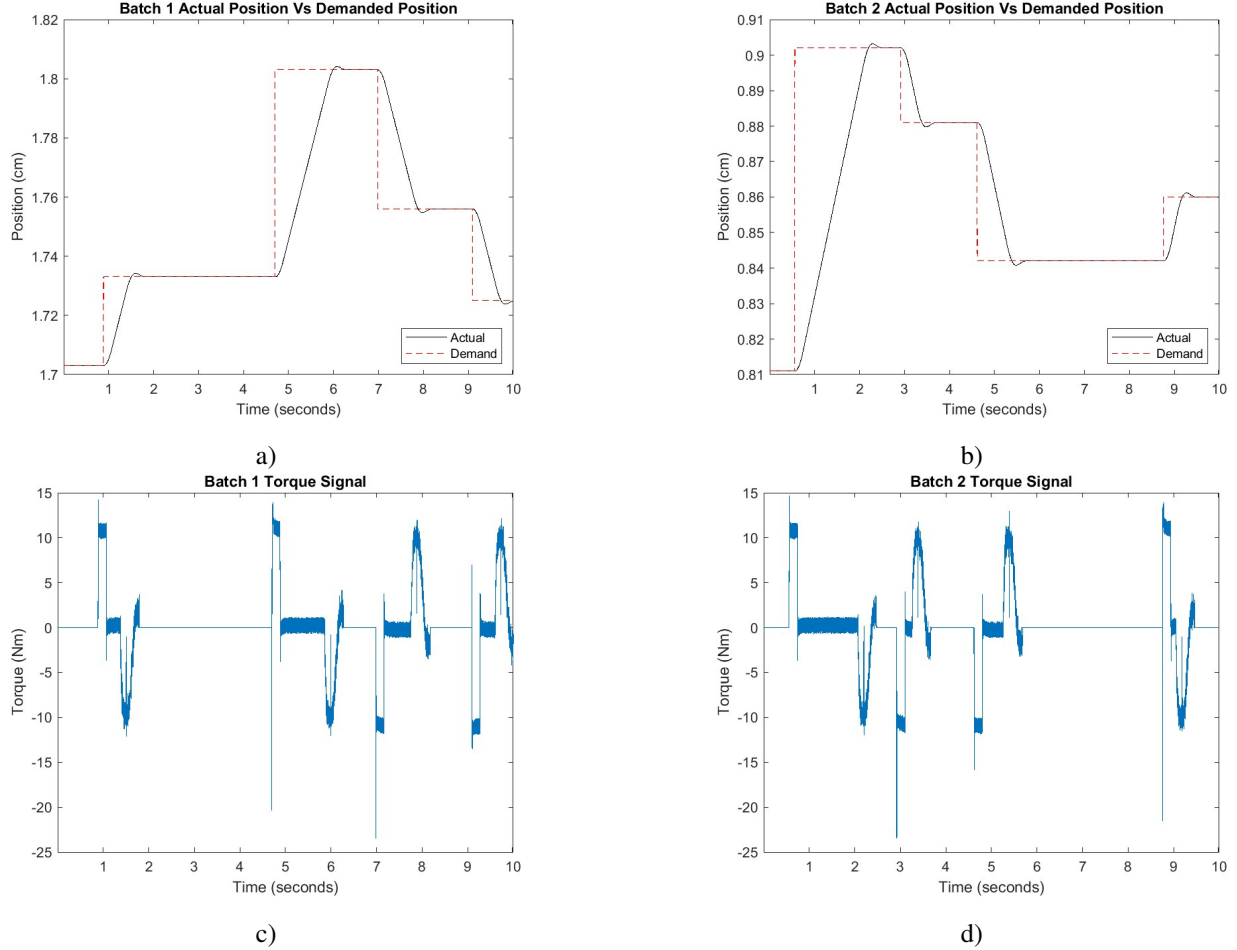


Figure 3. Position and torque profiles of single rods/servomotors in the healthy bank of a batch. a) - Batch 1 position; b) - Batch 2 position; c) - Batch 1 Torque; d) - Batch 2 torque

ing of the most important information in the data such as in autoencoders for denoising applications (Vincent et al., 2008) and image segmentation with the popular U-Net CNN structure (Yin et al., 2022). Since there are different types of faults in the faulty class, learning the most important information is useful for generalization within this class while differentiating it from the healthy class, hence, the E-D structure choice. This is also especially important since there are only a few examples in each class and data augmentation was not desired in this work. The final layer of the model has two dense neurons with a *softmax* activation function because there are two classes of interest here. An alternative would have been to have one output neuron with a *sigmoid* activation but the multiple neurons were chosen so that the model can be easily adapted for other tasks in this work. The employed network has about 18,400 trainable parameters which makes it relatively small given the complexity of the task and the limited data samples.

The first and most important step is to detect whether or not a fault has occurred in a control rod bank. As mentioned

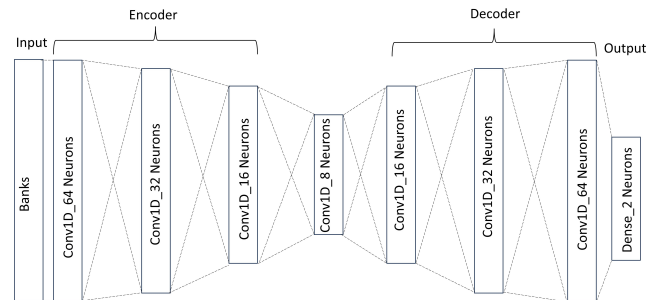


Figure 4. Model for detection tasks - Encoder-Decoder structure

in section 2, data is separated by fault type (Healthy/None, Short-Circuit, Ramp, and Step). There are twelve batches of data with four banks per batch and ten rods per bank. For the detection task, four tests were done; the first three involved having a faulty class that only included each of the three fault types, and a fourth test combined all the fault types in the faulty class. Confusion matrices were used to evaluate model

detection performance. For the different tests, the total data size varied but the split between training, validation, and final test sets were kept consistent at 70%, 15%, and 15% respectively. These splits were stratified to ensure proportionate representations from each class. For the individual fault detection tests, the total available data per sensed signal type was from twenty-four banks (twelve healthy and twelve faulty) whereas data from forty-eight banks were available for the combined fault tests (twelve healthy and twelve each for the three fault classes). Using displacement data has shown potential based on literature, where residuals between demanded positions and actual rod positions were monitored (Fullilove et al., 2022). However, in this research, good results were not obtained with position signals, so most of the results for this task and all other tasks place a firm focus on torque signals.

3.2. Fault Isolation

One way to isolate faults is to reconstruct inputs with a properly trained model while monitoring the deviation of these reconstructions (Cartocci et al., 2021; Yan et al., 2018) during tests. A model architecture that is highly employed for this purpose is the autoencoder (Liang et al., 2020), hence, its selection here. The isolation of faults was done by analyzing the errors of autoencoders that were trained to reconstruct the input banks. As a result, isolation was a regression task and the output layer was the same size as the input. Fig. 5 shows the employed model structure for the different tasks under this category and the small dimension of the latent space ('2') was selected because the relevant information in the data is expected to be captured by a few neurons since all the rods in a bank always move in the same way in response to the same position demand. The model has five hidden layers and 5,292 parameters making it a relatively small deep learning model.

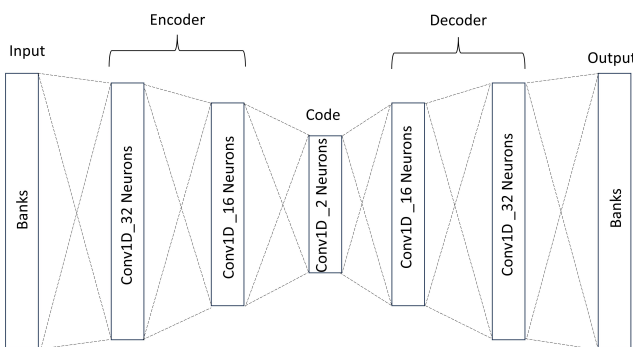


Figure 5. Autoencoder for the isolation tasks

For each of the different isolation tests done, the model was trained on the healthy data before predicting the faulty data (test set). The test was first done on a single batch which had 4 banks before testing with the twelve batches, multiple faults in a bank, and a varied number of rods in a bank. Reconstruction errors for each rod were compared by taking the

mean error across samples for each rod, and a noticeably high reconstruction error indicates a faulty rod. In other words, of all the rods, the maximum contributors to reconstruction error for all samples were identified as the faulty rods. This means that the model was simultaneously detecting the fault and isolating the faulty rod. For visualization and model evaluation, maximum contributor plots were generated.

3.2.1. Single Batch Tests

We prefer to manage the amount of data needed to train an accurate model, so the first tests tried to use single batches of data rather than all six together. For one of the batches tested, the reconstruction errors for each rod can be found in Fig. 13 in section 4. It was found that using data from a single batch is effective for finding all the faults but requires a long model training time, so we proceed by using all twelve batches together to effectively increase the sample size and potentially reduce training time.

3.2.2. Combined Batch Tests

For the next set of tests, all twelve batches were merged prior to processing, but otherwise, model training and testing were conducted as in the single batch test. The model used was also unchanged. The reconstruction errors when using all twelve batches are found in Fig. 15 in section 4. Because this technique was capable of detecting all fault types, testing was then conducted in order to optimize the process and expand its usefulness.

3.2.3. Detecting Multiple Faults

The first test of the previously trained model was to check the robustness of the system by providing data that has multiple faulty rods, including different fault types. Data from rods was reorganized in order to create a bank that contained both a Ramp Fault and a Step Fault. Additionally, a bank was created that had a faulty rod of each type. These multi-fault banks were fed into the trained model, which was able to highlight each of the faulty rods.

3.2.4. Minimizing Number of Rods

Finally, the limits of the model's capabilities were tested by providing fewer than ten (10) rods to train and test on. This was done by simply using only two or three rods from the combined twelve-batch data set. Of these rods, one belonged to the fault mode being tested (one of the three Faults), whereas the other one or two were healthy rods. These required building and training another model with the same structure as before but with adjusted input sizes. The reconstruction errors were then evaluated to see if the faulty rods could be identified.

3.3. Fault Diagnosis

With a faulty rod isolated, it can also be helpful to an operator to know the most likely type of fault present, given that there are different causes of faulty behavior. Diagnostics was also a classification task and a 1D-CNN-based classifier with seven hidden sequential layers was constructed to complete this task. The network was used to classify the rods in cases of single faults in a bank. It was a three-class classification since each bank was classified according to the class of its faulty rod. Subsequently, the problem was made a little more complicated as a four-class problem by including the healthy banks to serve as a backup detector so that any wrongly classified healthy bank could be captured. Fig. 6 shows the E-D structured classifier used but subjectively better results were obtained by first extracting features from the input data with an autoencoder (see Fig. 7). This additional encoding by the autoencoder with a latent dimension of '3' or '4', depending on the task performed, was expected to extract only the relevant information for distinguishing between the investigated classes. The layer used in the bank classifier before the output '*dense*' layer is the '*global_max_pooling*' layer in place of the more common '*flatten*' and '*max_pooling*' layers. The '*global_max_pooling*' layer was used with the assumption that less complicated features are required to distinguish between the banks of each class compared to distinguishing between rods. This choice of layer potentially makes the bank classifier model more computationally efficient. The output is a fully connected layer with three or four neurons, and the '*soft_max*' activation function to cater to the classes of interest. In terms of the input data, thirty-six banks were available for the three-class problem but all forty-eight banks were used for the four-class task. The training, validation, and test splits were in the same proportion as in the detection tasks.

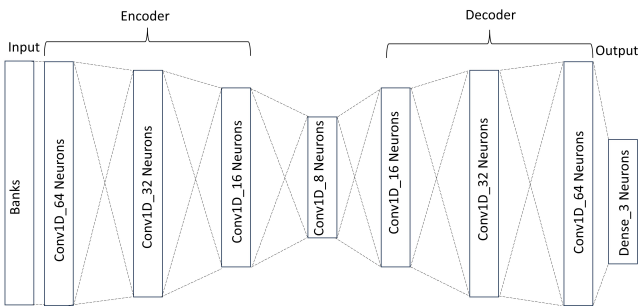


Figure 6. The fault classification model - Encoder-Decoder structure.

4. RESULTS

In this section, three types of figures are frequently used to display test outcomes. The bar charts show the distribution of contribution to the reconstruction error by each rod. If a bank is healthy, low values of reconstruction error are observed and the distribution is roughly even across the rods, indicating that

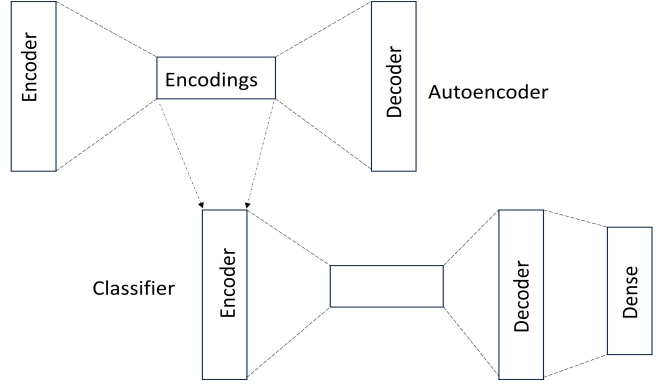


Figure 7. The diagnostics model with feature extraction from an autoencoder.

no particular rod is faulty. Faulty rods will have a noticeably higher reconstruction error than the other rods. The horizontal axis of these bar charts represents the different rods in the tested banks whereas the vertical axis is a measure of reconstruction error.

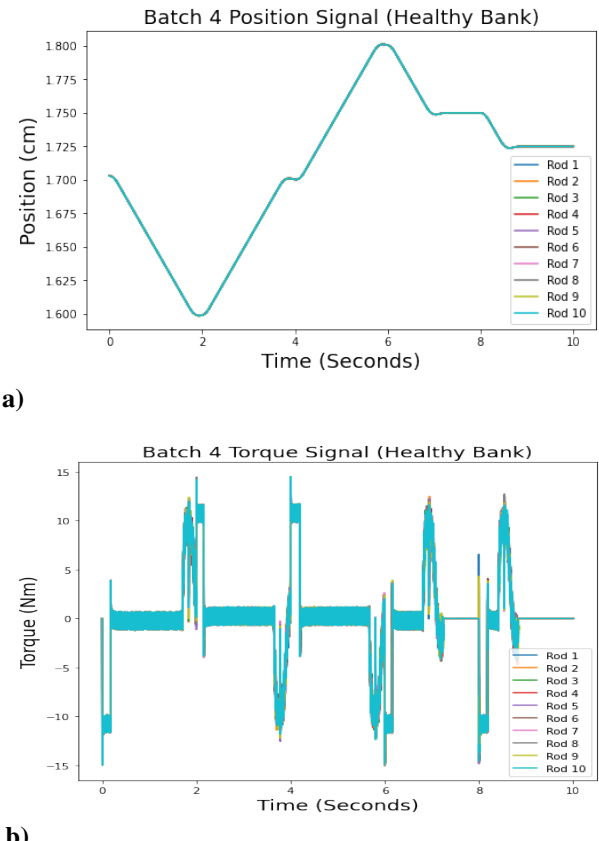


Figure 8. Monitored variables of the 10 rods in the healthy bank of batch '4'. a) - the position profile and b) - the torque profile of the bank.

To emphasize the isolation, a state classification (isolation)

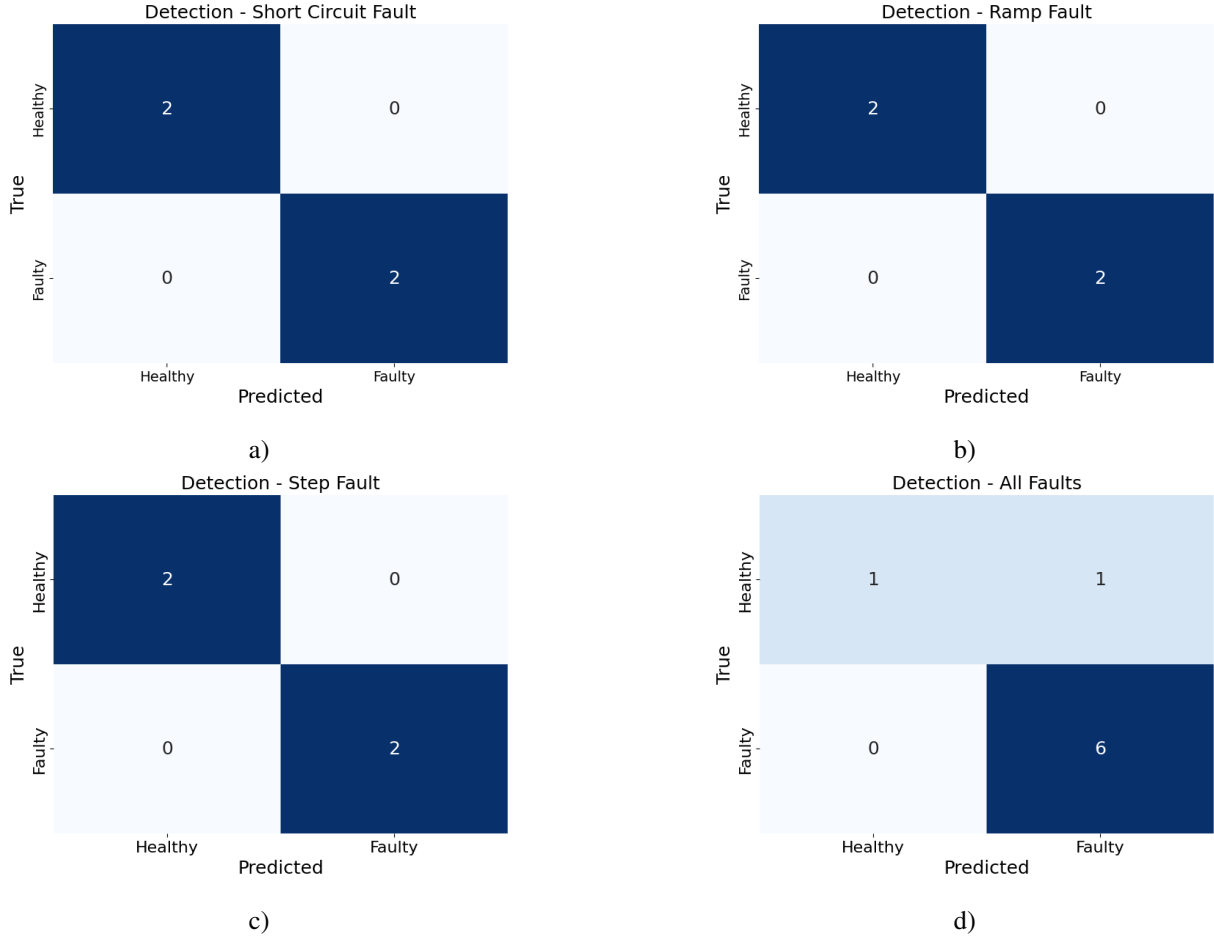


Figure 9. Fault detection with torque variable. a) Short-circuit Fault; b) Ramp Fault; c) Step Fault; d) All faults

plot was used to classify each rod in the tested banks as either faulty (class '1') or not (class '0'). The criterion for these state classifications is based on the reconstruction errors and is elucidated in section 4.3. For the detection and diagnostics tasks, confusion matrices were used to evaluate the results.

4.1. Data Inspection

The positions and torque values for all ten rod/motor combinations in the healthy bank of batch '4' are shown in Fig. 8. As expected for a healthy bank, all ten combinations behave similarly, leading to almost entirely overlapping data lines. The ten rods have the same position profile and the ten motors have the same torque profile. In this batch, changing demands caused the rods to move from their starting position at 1.7cm down to 1.6cm, then briefly back to 1.7cm before going up to 1.8cm, and so on. It can be seen that the spikes in torque correspond to the times at which movement is beginning or settling is occurring. These spikes in torque correspond to periods where the servomotors are being called to action and the periods of gradual rise or fall in positions correspond to active servomotor periods as explained in section

2. As seen, torque is more steady during active motor periods and around zero during non-active periods where a particular position is maintained for a prolonged period. These steady and zero-torque periods do not provide useful information for FDD tasks.

4.2. Detection

4.2.1. Torque Analysis

With torque, the classifier was able to consistently detect all the faults as shown in Fig. 9 where a), b), and c) show detections when the test sets only contain one type of fault in the faulty class. This was done to mimic realistic conditions where maintenance of only a specific fault type is of interest at the time. It also evaluates the model under conditions of class balance. In Fig. 9 d) all fault types are included in the faulty class and they were all correctly detected as faulty. One healthy bank was, however, incorrectly categorized as faulty. Although undesired, this is not detrimental since diagnostics will be carried out to check the fault types of the detected faults and including a 'no-fault' class in diagnostics

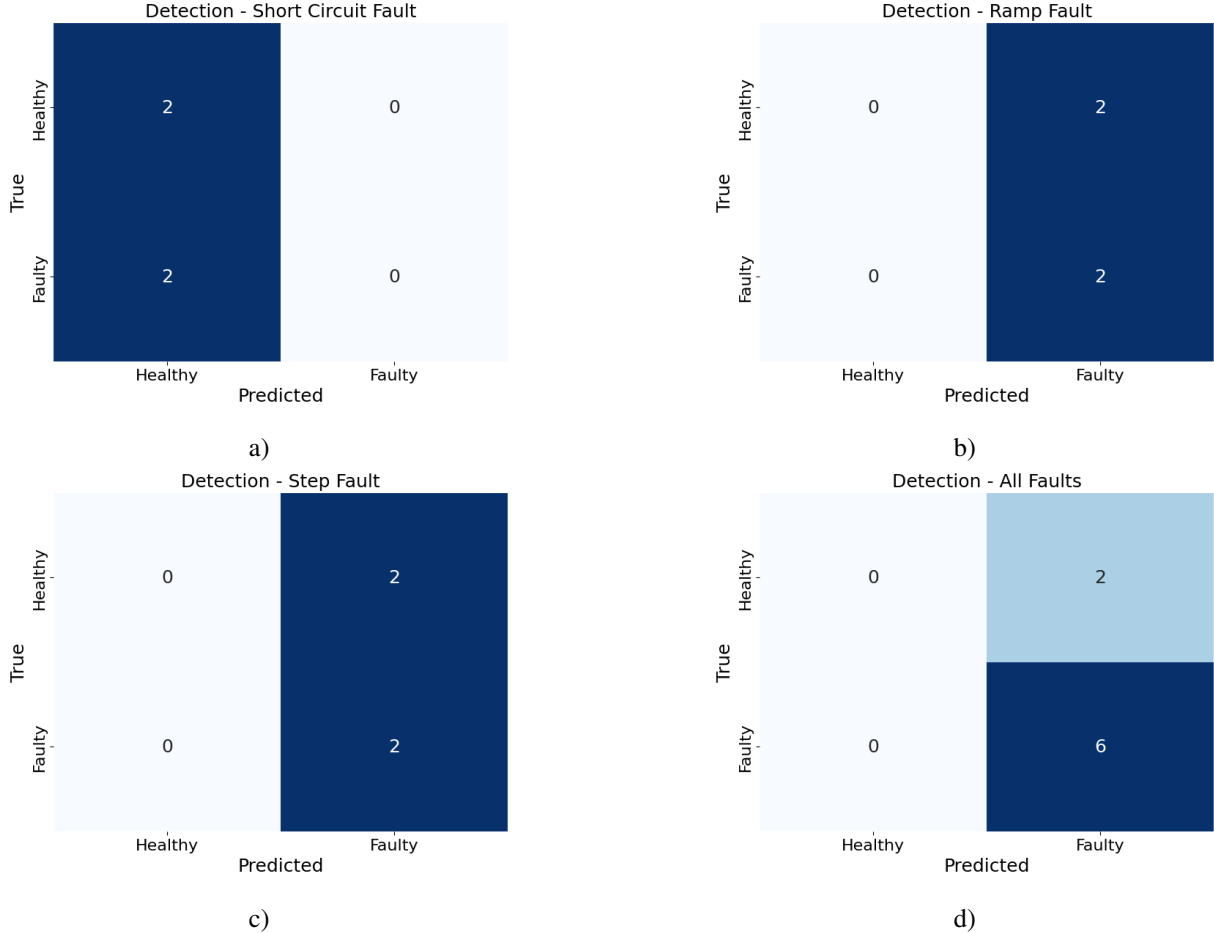


Figure 10. Fault detection with position variable to demonstrate that position is not suitable for the investigated system. a) Short-circuit Fault; b) Ramp Fault; c) Step Fault; d) All faults.

will capture the false detections. It would have been detrimental if a faulty bank were categorized as healthy since undetected faults could lead to bigger plant-wide problems that could further lead to prolonged loss of operations.

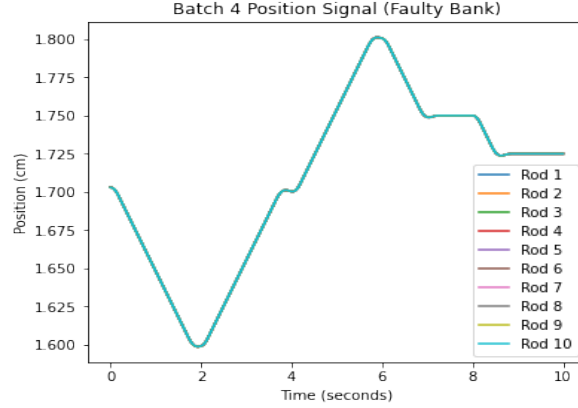
4.2.2. Position Analysis

Using the E-D structured classifier with positional data does not show a significant distinction between the healthy and the faulty banks. This can be seen in Fig. 10, where all the banks in a test set are classified as a single class. This indicates that the model is unable to learn to distinguish between a healthy rod and a faulty rod, so the position is unlikely to be a useful input for the model. It makes sense that this might be the case given that when inspecting the raw position data of a faulty bank (see Fig. 11 a)), it is indistinguishable from a healthy profile, and all rod displacements overlap entirely. A feedback control system that allows the rods to ride through faults to achieve the demanded positions was included in the simulated FMCRD system and is likely responsible for the observed characteristic in Fig. 11 a).

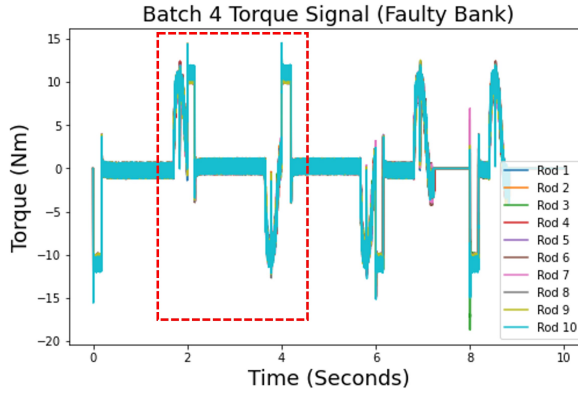
On the other hand, inspecting raw torque signals highlights a difference between the healthy and faulty torque profiles in the same batch. These differences occur mostly during the short spikes as expected and may appear subtle to the human eyes. Upon selecting a region of interest highlighted by the dashed line in Fig. 11 b), and zooming into the region, the differences become more apparent as indicated by the arrowheads in Fig. 12 where a shift in rod 10's torque signal is seen (same legend as in Fig. 11 b)). These subtle differences shown for a particular section are repeated throughout the observation period and are captured by the features learned by the employed deep learning models. As a result, all other tests are focused on the torque variable only.

4.3. Isolation

Two plot types were used to evaluate performance in this section: the fault contribution plot that displays the mean reconstruction error per rod across samples; and the fault isolation plot that identifies the faulty rods by simply predicting either '0' for no fault or '1' for a fault on each rod. The isolation



a)



b)

Figure 11. Position and torque profiles of a faulty bank in batch '4' with step fault. Dashed lines mark a region of interest. a) Position; b) Torque.

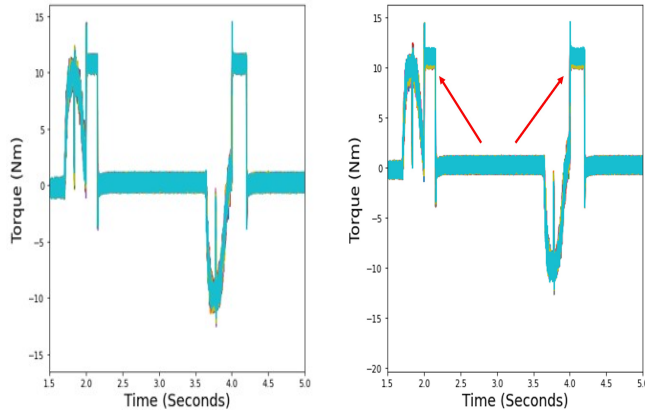


Figure 12. Zoomed in sections of the torque profiles of different banks in batch '4'. a) Healthy; b) Step Fault. Legend from Fig. 11 b) applies.

plot was created using a threshold-based rod classification approach. The threshold can be calculated as $threshold =$

$factor * MRE$ where MRE is the mean reconstruction error of the healthy validation bank. The $factor$ should be positive and greater than '1' meaning that a rod is isolated only if its reconstruction error is higher than the mean reconstruction error of the healthy bank's rods. The factors used to multiply the mean error of the healthy bank can be varied depending on the fault type or optimized to be the same across classes. However, in this study, any control rod in a given bank with a reconstruction error surpassing two times the median of that bank's errors was considered faulty. This method utilizes each test bank's median as the threshold for classification, providing a potentially more tailored criterion for isolating possible faults.

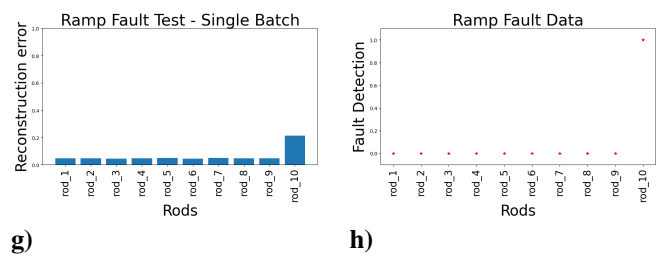
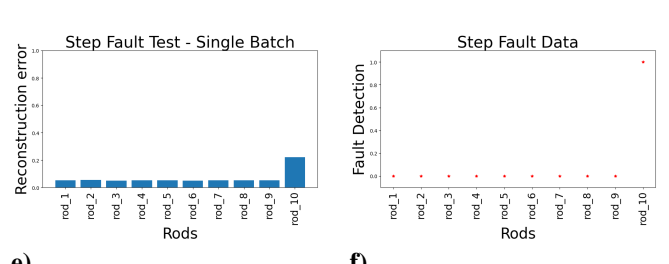
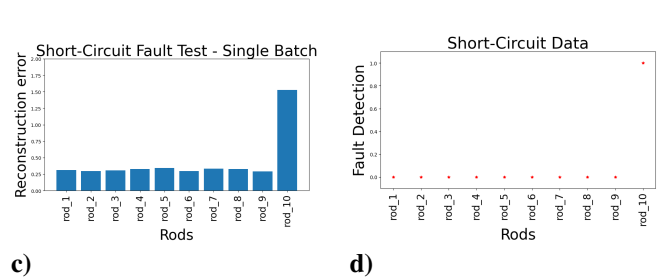
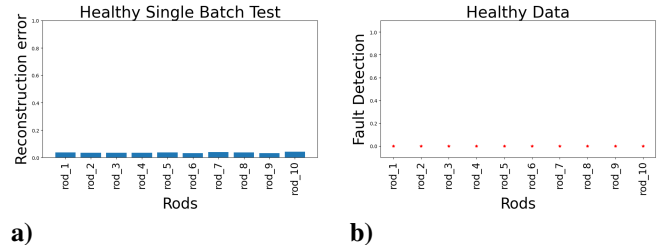


Figure 13. Fault isolation in a single batch with torque variable. Reconstruction error distributions are on the left and isolation plots are on the right. a) and b) - healthy; c) and d) - short circuit fault; e) and f) - step fault; g) and h) - ramp fault.

4.3.1. Single Batch Tests

Using torque data, a single batch is input into the model for training and testing. Since there is only one healthy bank in a batch, it was the sole training sample and no validation was used. The three faulty banks were then tested one after the other. Note that although results are only shown for batch '5', other batches have also been tested and produced very similar results.

When analyzing the data found in Fig. 13, it can be seen that the healthy data is processed correctly. All rods have similar reconstruction errors and as expected, no rod was isolated, both of which indicate a healthy bank. Additionally, the short fault output clearly shows a higher reconstruction error for rod 10 and a correct fault prediction, indicating a fault on rod 10. The correct rods were also isolated for the banks with step and ramp faults. This is an improvement on an existing statistical isolation method (Ifeanyi et al., 2023) since the current method required a sample with six times fewer data points to achieve the same consistent results.

4.3.2. Multiple Batch Tests

To adapt the model for a variety of applications, validating the training and setting thresholds with the reconstruction of the validation data is important. As a result, all the available healthy banks across all the batches were used for training the model. In this case, 9 samples were used for training and 3 samples for validation. The mean error of reconstructing the validation data was used to calculate the isolation thresholds of the test sets (faulty data). The loss profile of the model training is seen in Fig. 14 where convergence at a low loss value was quickly achieved around the 5th epoch. The validation loss closely followed the training loss, indicating that a stable and generalizable performance is expected from the model. The output from this test is found in Fig. 15.

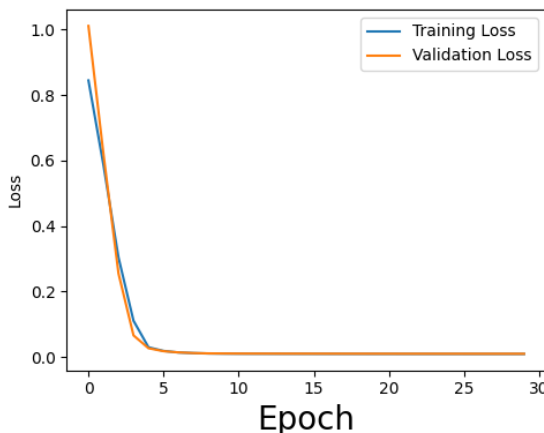


Figure 14. Loss profile of the model trained with multiple healthy samples

Looking at the reconstruction error plots indicates that the model is functional. The healthy data shows a low and very consistent error rate for all 10 rods, indicating no fault. The plots for the short fault and step fault show rod 10 as having a substantially higher reconstruction error than the other 9 rods, indicating a fault at that location. The output for the step fault also shows rod 10 as having a higher reconstruction error, meaning that the step fault is being detected and isolated. Additionally, the isolation plots all correctly identify the faulty rods.

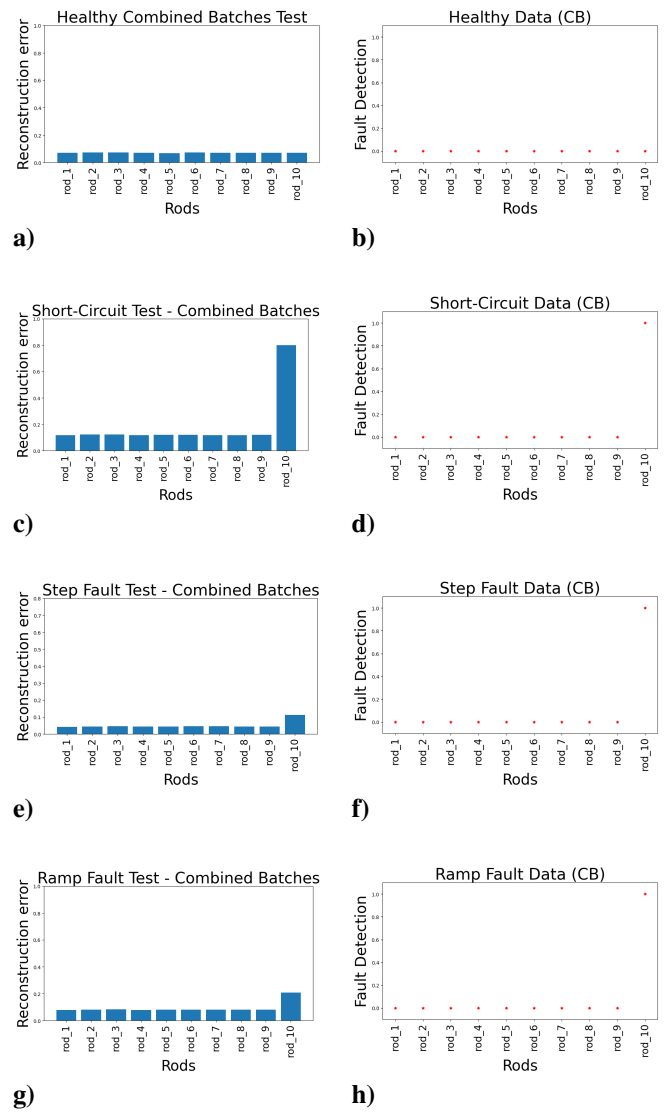


Figure 15. Fault isolation with multiple batches of torque variable. Reconstruction error distributions are on the left and fault isolation plots are on the right. a) and b) - healthy; c) and d) - short circuit fault; e) and f) - step fault, g) and h) - ramp fault. 'CB' stands for combined batches indicating that all the samples from all the batches were used for this test.

4.3.3. Isolating Multiple Faults

Given that the model is successful at finding a single faulty rod within a bank, the next step is to further test its capabilities by having it process a bank in which multiple rods are exhibiting faulty behavior. This is an important test because this scenario is possible in a real-world setting, and multiple faulty rods would be even more harmful to operations than a single faulty rod.

When there are two faulty rods in a bank, with the rod in position 5 being a ramp fault and the rod in position 10 being a step fault, the model does its detection and isolation jobs properly as shown in Fig. 16. The contribution plot shows the isolation in terms of reconstruction error whereas the isolation plot (right subplot) highlights the 2 anomalous rods in the bank. In other words, if an operator has identified a faulty bank and wants to know the anomalous rod/motor combination, this isolation plot may be used to narrow things down without necessarily showing reconstruction values which may be misleading due to the differences in error values for the different fault types.

Fig. 17 displays the performance of the autoencoder when all three fault types are present at different positions in a bank of rods. As seen, all three faults are correctly isolated to their sources, and the state classification plot further highlights the equal importance of all faults. For this task, the autoencoder isolated the faults better than the PCA approach (see Fig. 18) previously applied (Ifeanyi et al., 2023) in literature where T^2 statistics was monitored to detect and isolate faults. From the statistical approach, it was difficult to isolate the step fault in rod '4'. The isolation of multiple faults from the statistical method might have performed worse because the statistical model treats each observation of the sequence as independent which could lead to loss of vital temporal information. For the PCA method, all six banks were treated as one long sample with six times the observation period used in this current research so the model was focused on identifying one maximum contributor to fault.

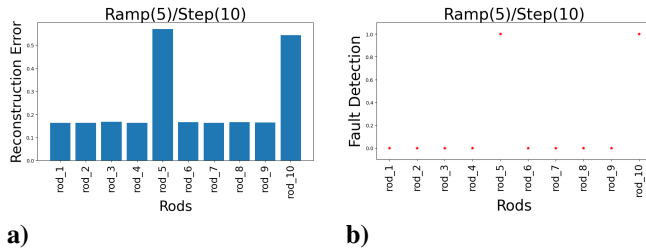


Figure 16. Ramp fault on rod 5 and step fault on rod 10

4.3.4. Minimizing Number of Rods

It is not usually the case in nuclear reactors that control rod banks will contain 10 rods so it is important to test the per-

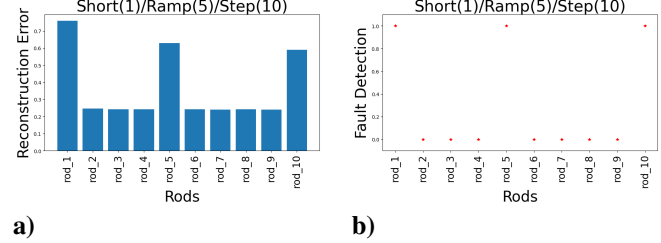


Figure 17. Short fault on rod 1, ramp fault on rod 5, step fault on rod 10

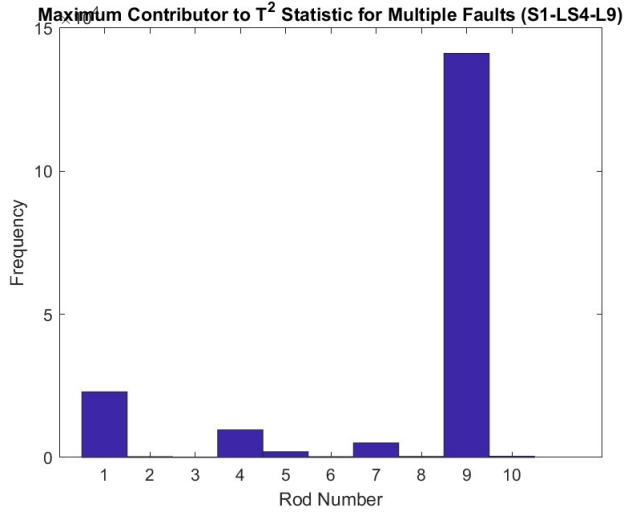


Figure 18. Results from a statistical approach for multiple faults in a bank. S - short-circuit (rod 1); L - ramp (rod 9); LS - step (rod 4).

formance of the proposed approach in cases where there are fewer rods. Given that there are fewer variables involved, the model was adjusted to have a latent dimension of 1 rather than 2.

Fig. 19 shows the fault isolation capability of the autoencoder approach where there are 3 rods with the faulty rods located at rod 3. As seen, reconstruction errors are consistent in the Healthy batch whereas all fault types are detected and correctly isolated. As in previous tests, the Step Fault is the hardest to detect.

When there are only 2 variables, it becomes difficult for the model to differentiate between faulty and healthy rod/motor combinations, as shown in Fig. 20. This is probably because the latent dimension is encoding more information than necessary for the discernment of the 2 variables and as a result, adds noise to the prediction.

The better fault detection performance from monitoring torque as opposed to position signals may be because of the direct relationship between current and torque. Motor Current Signature Analysis (MCSA), where the parameter changes of the

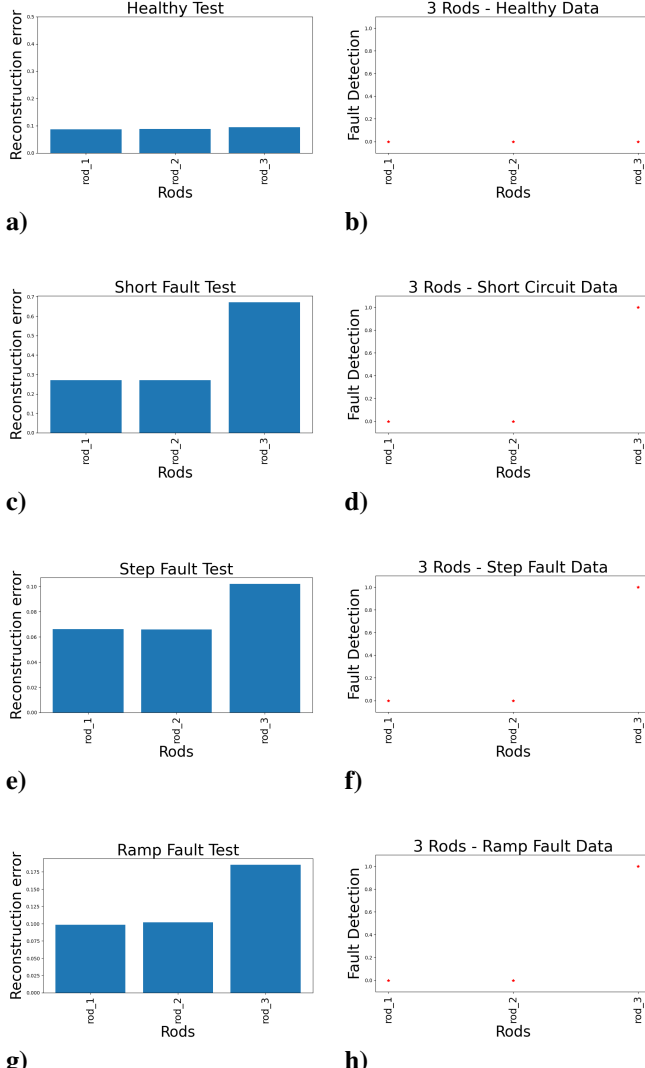


Figure 19. Three rods in a bank. a) and b) - healthy; c) and d) - short circuit fault; e) and f) - step fault, g) and h) - ramp fault.

current signals are investigated to detect system flaws, is the most used technique for fault detection and diagnostics of motors in the nuclear sector. Torque is more likely to exhibit these property changes in the current signal, which might account for the excellent torque performance as a variable. The poor performance of the position signal, on the other hand, is likely due to the ride-through capability and feedback control of the simulated drive mechanism which tries to ensure that the rods achieve their desired position even when faulty.

4.4. Fault Diagnostics

Other methods have been proposed for fault detection in a bank so it becomes reasonable to subject only the faulty banks to the identification test. The banks tested in this section contain only one faulty rod. Using the E-D structured classifier,

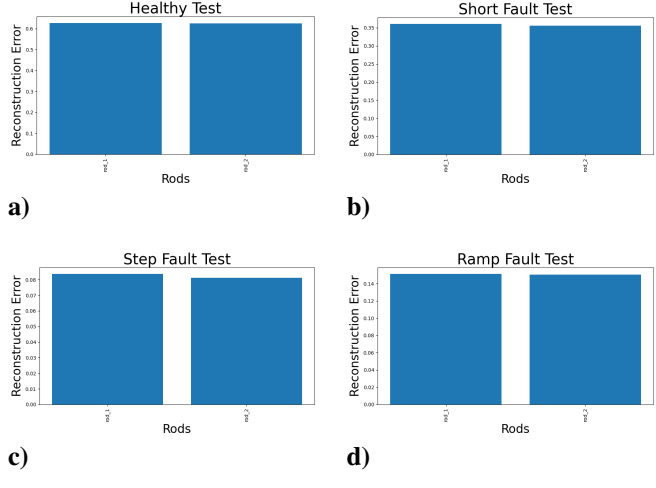


Figure 20. Two rods in a bank. a) - healthy; b) - short fault; c) - step fault; d) - ramp fault.

short-circuit and step faults were correctly diagnosed whereas one bank with ramp fault was misclassified as a short-circuit fault (see Fig. 21). This is highly undesirable since this is a misclassification of a mechanical fault as an electrical one and therefore directs maintenance to the wrong component.

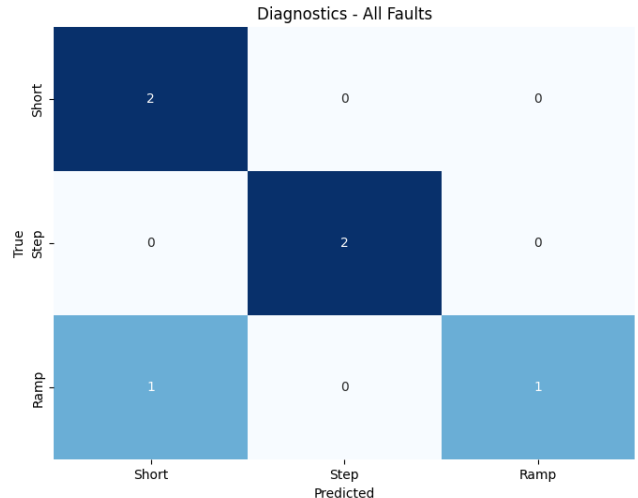


Figure 21. Fault diagnosis of 3 classes with E-D structured classifier

Since a highly undesired result was observed with the E-D structured classifier alone, an autoencoder was attached to the classifier (see Fig. 7) to potentially extract useful information from the input data before classification. The latent dimension of the autoencoder is '3' and the result of this diagnostics is shown in Fig. 22. In this case, there is still a misclassification of ramp fault as step fault making the accuracy of prediction the same as in the previous case but this misclas-

sification is slightly more desirable than in the previous case without the autoencoder. This is because the fault is still correctly identified as a mechanical fault and maintenance will be directed to the appropriate components.

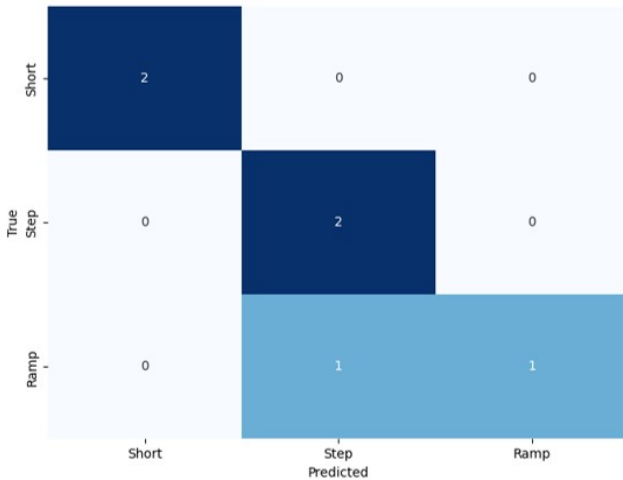


Figure 22. Fault diagnosis of 3 classes with autoencoder-fed E-D structured classifier

During detection, it was observed that one healthy bank was classified as faulty, so it is necessary to be able to handle this detection scenario during diagnostics by including the 'no fault' or healthy class in the diagnostics. The autoencoder-fed classifier was used for this task with a latent dimension of '4' and the result is shown in Fig. 23. In this case, all the healthy banks were correctly diagnosed as desired and the rest of the results are similar to the three-class task.

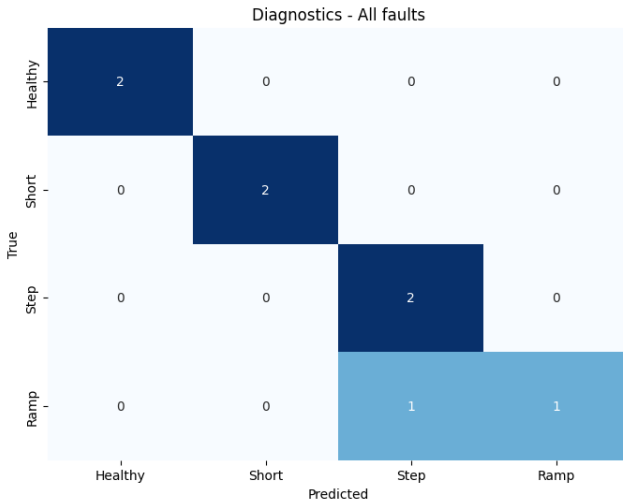


Figure 23. Fault diagnosis of 4 classes with autoencoder-fed E-D structured classifier

Overall, the proposed diagnostics technique successfully di-

agnosed all faults with the ramp fault being the most difficult to diagnose. This difficulty is possibly due to the slow build-up of the fault over time making it more subtle and harder to differentiate, especially with the intermittency of the system.

5. CONCLUSION

By using single and multiple batches of torque data to train an autoencoder, analyzing the reconstruction errors of data for each rod in a bank of FMCRD servomotors allows for the accurate isolation of both mechanical and electrical faults in this highly underinvestigated CRD system. The detection and isolation system is capable of determining the individual servomotor that is functioning abnormally and can even isolate multiple servomotors exhibiting different types of faults. Fault isolation continues to function with as few as three control rods in a bank.

The autoencoder can more easily isolate electrical faults than mechanical faults, in agreement with most methods employed in the literature. The autoencoder, however, was capable of isolating both electrical and mechanical faults. The easier isolation of the electrical fault might be due to the low magnitude of the step fault and the small gradient of the ramp fault. Perhaps higher fault magnitude and gradients would make them more perceptible to the model. To more easily capture mechanical faults, it might be worth considering the addition of torque sensors or sensors for measuring similar properties in the BWRX-300 SMR.

As for fault type diagnostics, the results are promising using the torque data. The employed approach worked reasonably well when there was a single fault in a bank. Diagnosing banks of multiple faults is an area that will be investigated in the future.

For other future works, a different training strategy that would focus on optimizing a model metric such as the F1 score or Area under the receiver operating characteristics curve (AUC-ROC) could be employed to improve detection performance for this imbalanced scenario. These metrics inherently take the imbalance of the classes into account as opposed to the accuracy metric optimized in this work.

ACKNOWLEDGMENT

The information, data, or work presented herein was funded in part by the Advanced Research Projects Agency-Energy (ARPA-E), U.S. Department of Energy, under Award Number DE-AR0001290. The views and opinions of authors expressed herein do not necessarily state or reflect those of the United States Government or any agency thereof.

REFERENCES

Ahmed, S. F., Alam, M. S. B., Hassan, M., Rozbu, M. R.,

- Ishtiaq, T., Rafa, N., ... Gandomi, A. H. (2023). Deep learning modelling techniques: current progress, applications, advantages, and challenges. *Artificial Intelligence Review*, 1–97.
- AP News. (Accessed: Oct. 19, 2023). *1st small modular nuclear reactor certified for use in US*. Retrieved from <https://apnews.com/article/us-nuclear-regulatory-commission-oregon-climate-and-environment-business-design-e5c54435f973ca32759afe5904bf96ac>
- Azizjon, M., Jumabek, A., & Kim, W. (2020). 1d cnn based network intrusion detection with normalization on imbalanced data. In *2020 international conference on artificial intelligence in information and communication (icaaic)* (pp. 218–224).
- Cartocci, N., Napolitano, M. R., Costante, G., & Fravolini, M. L. (2021). A comprehensive case study of data-driven methods for robust aircraft sensor fault isolation. *Sensors*, 21(5), 1645.
- Chalapathy, R., & Chawla, S. (2019). Deep learning for anomaly detection: A survey. *arXiv preprint arXiv:1901.03407*.
- Chandola, V., & Banerjee, A. (n.d.). V., k.(2009). anomaly detection: A survey. *ACM Computing survey*, 41.
- Chen, Z., Yeo, C. K., Lee, B. S., & Lau, C. T. (2018). Autoencoder-based network anomaly detection. In *2018 wireless telecommunications symposium (wts)* (pp. 1–5).
- Energy.gov. (Accessed: Oct. 19, 2023). *NRC Certifies First U.S. Small Modular Reactor Design*. Retrieved from <https://www.energy.gov/ne/articles/nrc-certifies-first-us-small-modular-reactor-design>
- Eren, L., Ince, T., & Kiranyaz, S. (2019). A generic intelligent bearing fault diagnosis system using compact adaptive 1d cnn classifier. *Journal of Signal Processing Systems*, 91, 179–189.
- Fullilove, N., Dos Santos, D., Saxena, A., & Coble, J. (2022). Leveraging within-bank comparison for anomaly detection, diagnostics, and prognostics in advanced nuclear power plants. In *Annual conference of the phm society* (Vol. 14).
- Givnan, S., Chalmers, C., Fergus, P., Ortega-Martorell, S., & Whalley, T. (2022). Anomaly detection using autoencoder reconstruction upon industrial motors. *Sensors*, 22(9), 3166.
- Goodge, A., Hooi, B., Ng, S. K., & Ng, W. S. (2021). Robustness of autoencoders for anomaly detection under adversarial impact. In *Proceedings of the twenty-ninth international conference on international joint conferences on artificial intelligence* (pp. 1244–1250).
- Ifeanyi, A., Saxena, A., & Coble, J. (2023). Within-bank condition monitoring and fault detection of fine motion control rod drives. *13th Nuclear Plant Instrumentation, Control & Human-Machine Interface Technologies (NPIC&HMIT 2023)*, 66(8), 1053–1062.
- Jie, Z., Cuiyun, P., Pan, H., & Caixue, L. (2019). Research on current monitoring and fault diagnosis technology for control rod drive mechanism. *核动力工程*, 40(1), 172–175.
- Jung, J.-H., Lee, J.-J., & Kwon, B.-H. (2006). Online diagnosis of induction motors using mcsa. *IEEE Transactions on Industrial Electronics*, 53(6), 1842–1852.
- Kowalski, C. T., & Orlowska-Kowalska, T. (2003). Neural networks application for induction motor faults diagnosis. *Mathematics and computers in simulation*, 63(3–5), 435–448.
- Liang, X., Duan, F., Bennett, I., & Mba, D. (2020). A sparse autoencoder-based unsupervised scheme for pump fault detection and isolation. *Applied Sciences*, 10(19), 6789.
- Louis, H. K., Refeat, R. M., & Hassan, M. I. (2021). Control rod shadowing effect in pwr core utilizing urania-gadolinia fuel. *Progress in Nuclear Energy*, 142, 103993.
- Mehala, N., & Dahiya, R. (2007). Motor current signature analysis and its applications in induction motor fault diagnosis. *International journal of systems applications, engineering & development*, 2(1), 29–35.
- Messaoudi, M., & Sbita, L. (2010). Multiple faults diagnosis in induction motor using the mcsa method. *International Journal of Signal & Image Processing*, 1(3).
- Rezaeianjouybari, B., & Shang, Y. (2020). Deep learning for prognostics and health management: State of the art, challenges, and opportunities. *Measurement*, 163, 107929.
- Shim, J., Lim, G. C., & Ha, J.-I. (2022). Unsupervised anomaly detection for electric drives based on variational auto-encoder. In *2022 ieee applied power electronics conference and exposition (apec)* (pp. 1703–1708).
- Subramanian, A., Saxena, A., & Coble, J. (2023). Servo-motor dataset: Modeling health in mechanisms with typically intermittent operation. In *Annual conference of the phm society* (Vol. 15). doi: 10.36001/phm-conf.2023.v15i1.3580
- Tang, W., Long, G., Liu, L., Zhou, T., Jiang, J., & Blumenstein, M. (2020). Rethinking 1d-cnn for time series classification: A stronger baseline. *arXiv preprint arXiv:2002.10061*, 1–7.
- Vincent, P., Larochelle, H., Bengio, Y., & Manzagol, P.-A. (2008). Extracting and composing robust features with denoising autoencoders. In *Proceedings of the 25th international conference on machine learning* (pp. 1096–1103).
- Yan, Z., Yao, Y., Huang, T.-B., & Wong, Y.-S. (2018). Reconstruction-based multivariate process fault isolation using bayesian lasso. *Industrial & Engineering*

- Chemistry Research*, 57(30), 9779–9787.
- Yin, X.-X., Sun, L., Fu, Y., Lu, R., Zhang, Y., et al. (2022). U-net-based medical image segmentation. *Journal of Healthcare Engineering*, 2022.
- Zhongming, Y., & Bin, W. (2000). A review on induction motor online fault diagnosis. In *Proceedings ipemc 2000. third international power electronics and motion control conference (ieee cat. no. 00ex435)* (Vol. 3, pp. 1353–1358).

BIOGRAPHIES



Ark O. Ifeanyi graduated from the University of Benin, Nigeria with a B.Eng. in Electrical and Electronic Engineering in 2016 before obtaining an MSc. in Renewable Energy Systems Technology from Loughborough University, Leicestershire, UK in 2020. He joined the Bredesen Centre for Interdisciplinary Research and Graduate Education at the University of Tennessee, Knoxville, in the Spring of 2022 and is currently pursuing a Ph.D. in Energy Science and Engineering. His current research is focused on the application of machine learning and artificial intelligence to the Prognostics and Health Management (PHM) of nuclear plants including small modular reactors (SMRs). Specifically, he is developing advanced machine learning algorithms to detect and diagnose faults in nuclear power plants, with the ultimate goal of improving the safety, reliability, and efficiency of nuclear energy production.

Member - Institute of Electrical and Electronics Engineers (IEEE); Student Member - American Nuclear Society (ANS); Chevening Scholar - 2019; Bredesen Center Fellow - 2021.

Abhinav Saxena is a Principal Scientist in AI & Learning Systems at GE Research. He has been developing ML/AI-based PHM solutions for various industrial systems (aviation,

nuclear, power, and healthcare) at GE and has been driving the integration of AI-based PHM analytics in GE's industrial systems. He is the PI for ARPA-E GEMINA program led by GE Research on AI-Enabled Predictive Maintenance Digital twins for Advanced Nuclear Reactors. Abhinav is also an adjunct professor in the Division of Operation and Maintenance Engineering at Lulea University of Technology, Sweden. Prior to GE, He was a Research Scientist with SGT Inc. at NASA Ames Research Center for over seven years. His interests lie in developing PHM methods and algorithms with special emphasis on deep learning and data-driven methods in general for practical prognostics. He has published over 100 peer-reviewed technical papers and has co-authored a seminal book on prognostics.

He actively participates in several SAE standards committees, IEEE prognostics standards committee, and various PHM Society educational activities, and is a Fellow of the PHM Society. He also served as chief editor of the International Journal of Prognostics and Health Management between 2011-2020. Abhinav actively participates in the organization of PHM Society conferences and various AI workshops on topics of Digital Twins and AI in Industrial applications.

Jamie B. Coble is an Associate Professor of Nuclear Engineering at the University of Tennessee, Knoxville (UTK). She earned her Ph.D. in Nuclear Engineering in 2010 from UTK. Prior to joining the faculty, she was a scientist in the Applied Physics group at Pacific Northwest National Laboratory. Her research interests lie mainly in applications of data analytics and machine learning in operations and maintenance of nuclear power plants. She is a member of American Nuclear Society and U.S. Women in Nuclear, senior member of IEEE, and fellow of the Prognostics and Health Management Society and of the International Society of Engineering Asset Management.